Supramolecular Control of Two-Dimensional Phase Behavior

Steven De Feyter,*[a] Mattias Larsson,[a, c] Norbert Schuurmans,[b] Bas Verkuijl,[b] George Zoriniants,[a] André Gesquière,[a] Mohamed M. Abdel-Mottaleb,[a] Jan van Esch,*[b] Ben L. Feringa,[b] Jan van Stam,[c] and Frans De Schryver[a]

Abstract: We have used directed two-component self-assembly to "pattern" organic monolayers on the nanometer scale at the liquid/solid interface. The ability of the scanning tunneling microscope to investigate structural details in these adlayers was used to gain insight into the two-component two-dimensional phase behavior. The components are symmetrically alkylated bisurea derivatives (R1-urea-spacer-urea-R2; R1, R2 = alkyl, spacer = alkyl or bisthiophene). The bisthiophene unit acts as a marker and its bisurea derivative (**T2**) is a component in all the mixtures investigated. By varying the position of the hydrogen-bond forming urea groups along the molecule and the length of the alkyl chains of the other components, the effect of 1) hydrogen bonding, 2) molecule length, 3) odd – even effects, and 4) shape complementarity on the two-dimensional phase behavior was investigated. Insight into the effect of these parameters leads to the control of the two-dimensional patterning: from randomly intermixed systems to phase separation.

Keywords: monolayers · physisorption · scanning probe microscopy · self-assembly

Introduction

The control of the lateral assembly and spatial arrangement of micro- and nano-objects at interfaces is a prerequisite when it comes to potential applications in the field of nanoscience and technology. To create two-dimensional patterns, one can take advantage of "active" manipulation techniques, such as photolithography, electron beam lithography,[1] and "soft lithography".[2] Scanning probe microscopy (SPM) techniques, such as scanning tunneling microscopy (STM) and atomic force microscopy (AFM), are another class of techniques that can be implemented for the controlled manipulation of matter.[3–9]

Self-assembly methods provide an alternative approach to make defined structures with dimensions on the nanometer scale. Self-assembly is a natural phenomenon that can be observed in many biological, chemical, and physical processes.[10] Self-assembled monolayers (SAMs) are ordered molecular assemblies formed by the adsorption of an active surfactant on a solid surface.[11] Many SAMs have been investigated, but monolayers of alkane thiolates on gold are the most popular ones. Several groups have taken advantage of the spontaneous formation of SAMs and the formation of nanometer-sized domains by the coadsorption of two or more adsorbates.[12, 13] If more than one adsorbate is involved in the self-assembly process, one must consider the interactions between the different components. STM and AFM proved to be useful in identifying phase separation on the nanometer scale.[13, 14] In studies involving mixtures of molecules differing only in the nature of the end groups, it was shown that the difference in their polarity drives the extent of phase separation.[15] In addition to phase separation induced by differences in the alkyl chain length,[14] it was demonstrated that phase separation can be driven by intermolecular interactions buried within the film.[16]

Less attention has been given to the self-assembly of physisorbed layers at surfaces. In contrast to chemisorbed structures, physisorption is not very suitable for making "permanent" architectures. Nevertheless, these physisorbed adlayers are model systems to investigate the interplay between molecular structure and the formation of ordered assemblies in two dimensions and can be studied in great detail with STM.[17–21] A very convenient method for the formation of extended 2D structures is physisorption at the liquid/solid interface.[22, 23] The preparation is relatively simple, and STM allows a detailed investigation of the two-dimensional patterns.[24–27] However, it still remains a chal-

[a] Dr. S. De Feyter, M. Larsson, Dr. G. Zoriniants, Dr. A. Gesquière, Drs. M. M. Abdel-Mottaleb, Prof. F. De Schryver
Katholieke Universiteit Leuven, Departement Scheikunde
Celestijnenlaan 200 F, 3001 Leuven (Belgium)
Fax: (+32) 16-327989
E-mail: steven.defeyter@chem.kuleuven.ac.be

[b] Dr. J. van Esch, Drs. N. Schuurmans, B. Verkuijl, Prof. B. L. Feringa
University of Groningen, Material Science Center, Stratingh Institute
Laboratory of Organic and Inorganic Molecular Chemistry
Nijenborg 4, 9747 AG Groningen (The Netherlands)
E-mail: j.van.esch@chem.rug.nl

[c] M. Larsson, Prof. J. van Stam

0947-6539/03/0905-1198 $ 20.00+.50/0

lenge to control the ordering in multicomponent mixtures at the supramolecular level. Most binary mixtures investigated so far show phase separation on the nanometer scale[28–33] or the formation of randomly mixed monolayers.[34–41] Highly ordered bimolecular two-dimensional adlayers are only formed in a few cases.[42–49]

Recently, we found that simple alkyl and oligothiophene bisurea compounds can form mixed bimolecular adlayers, and we have exploited this feature to study the electronic properties of the oligothiophene moieties and its supramolecular arrays by means of tunneling spectroscopy.[50] The different contrast from the thiophene and alkyl moieties greatly facilitates the observation of phase-separated or mixed adlayers, and this feature was used to study pattern formation in physisorbed adlayers of bimolecular mixtures of alkyl and thiophene bisurea compounds on graphite in more detail. Here we report on the results of these studies, in which we address the interplay between molecular structure, supramolecular interactions, and occurrence of phase separation or mixing in two-dimensional monolayers. The results clearly show that it is possible to direct pattern formation in monolayers via intermolecular interactions, which will be exploited in future studies on the patterning of two-dimensional monolayers at the supramolecular level.

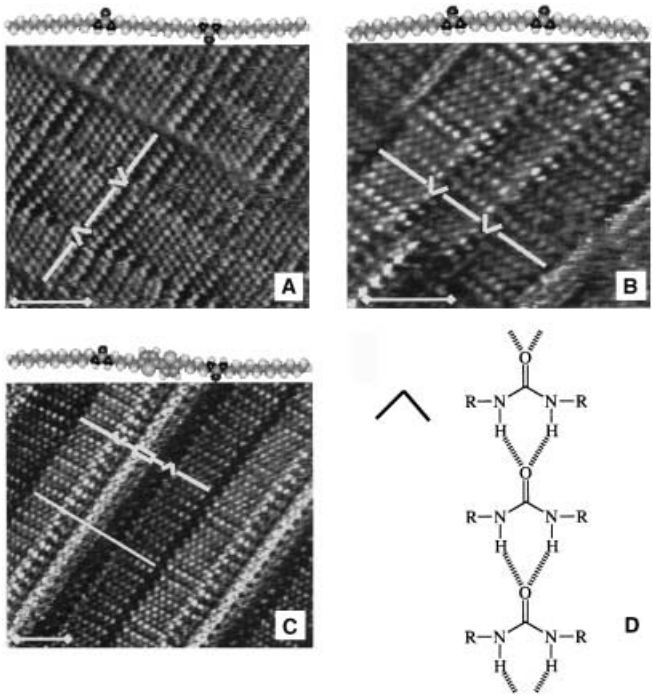

Figure 1. STM images reflecting the ordering of the bisurea derivatives in monocomponent systems. A) **C12-12**, B) **C9-12**, C) **T2**. The inset (top) shows a molecular model based upon semiempirical calculations. The same symbols as in Figure 4 are used, a few molecules are indicated. D) Hydrogen-bonding pattern of urea groups. The scale bar measures 2 nm. The difference in contrast between the urea groups in C is attributed to a scanning artefact.[45]

Results and Discussion

The compounds investigated are alkylated bisurea derivatives (Scheme 1), which are known to assemble efficiently at the liquid/solid interface (Figure 1).[50–53] These molecules physisorb on the graphite substrate with their long molecular axis parallel to the substrate while forming extended tapes or lamellae. In monocomponent monolayers, the dominating intermolecular interaction is the formation of hydrogen bonds between the urea groups (Figure 1 D). Within a tape, each molecule is stabilized by eight hydrogen bonds, which determines the intermolecular distance of 0.46 nm. As a result, it was shown that, in the case of **T2** (Scheme 1), the thiophene rings are tilted with respect to the graphite substrate. This allows the possibility of $\pi-\pi$ interactions between adjacent molecules in a stack.[50] The thiophene rings can easily be recognized as the brightest spots in the images; this is caused by the enhanced tunneling current associated with them. The alkyl chains appear less bright. In **CX-Y**-type molecules (Scheme 1), the contrast associated with the urea groups is often quite different from the alkyl chains so that they can be easily located (Figure 1). In **T2** molecules, this is often more difficult because of the adjacent "bright" bisthiophene groups.

The number of carbon atoms of the alkyl group linking both urea groups (called "spacer"), being odd or even, determines the shape of the molecule. If the number of carbon atoms is even the molecule adopts an extended "zigzag" shape, with the urea groups pointing in opposite directions. If the alkyl spacer contains an odd number of carbon atoms, the molecule is "bow"-shaped, and the urea

T2

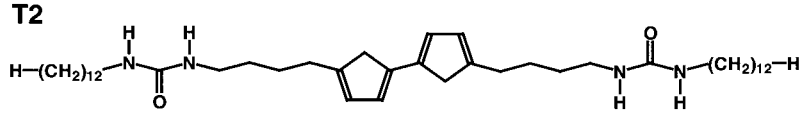

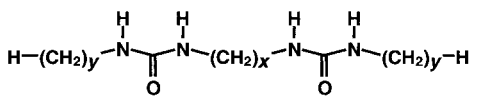

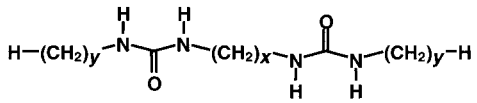

Cx-y	x	y
C9-12	9	12
C15-12	15	12
C9-15	9	15
C6-12	6	12
C8-15	8	15
C12-12	12	12
C14-12	14	12
C14-6	14	6
C16-12	16	12

Scheme 1. Chemical structures of the bisthiophene derivative (**T2**) and the other derivatives containing bisurea (**CX-Y**) used as coadsorbents. The two different chemical structures shown for **CX-Y** relate to the effect of the number of methylene groups connecting both urea groups: upper one (odd), lower one (even).

  0947-6539/03/0905-1199 $ 20.00+.50/0

groups point in the same direction. This is illustrated in Figure 1A, B.

Variation of alkyl spacer length

In a first series of experiments, the spacer length—the alkyl chain connecting both urea groups—was varied systematically and its effect on the mixing behavior was studied by STM. The length of the outermost alkyl chains (dodecyl side chain) is kept constant and is identical to those of the **T2** molecules. **T2** was mixed with **Cx-12** (where $x = 6$, 9, 12, 14, 15, or 16) in a 1:1 molar ratio and the composition of the mixed monolayers was studied at the HOPG/1-octanol interface. In good agreement with the studies of the pure compounds, the mixtures form monolayers composed of tapes (Figures 2 and 3). Within the monolayers, the **T2** molecules are easily identified by the appearance of the bright features located in the center of the tapes, corresponding to the location of the bisthiophene moieties. The molecules are lying "flat" on the HOPG surface and adopt a fully extended conformation. The intermolecular distance measures 0.46 nm.

T2/C6-12: In **T2/C6-12** mixtures (Figure 2A, B) exclusively microphase separation occurs into **T2** and **C6-12** blocks. From a practical point of view, phase separation is defined to reflect those situations where (almost) all **T2** blocks consist of more than five **T2** molecules. Pure **T2** and **C6-12** blocks are formed; however, they are not ordered in a random way. They are in line and at one side of the lamellae, the dodecylurea groups are in registry. At the boundary between two blocks, this "fit" allows hydrogen bonding between **T2** and **C6-12** molecules, given that the orientation of the urea groups is the same (model Figure 4A).

T2/C14-12: If **T2** is mixed with **C14-12**, which is identical in size including the spacer connecting the urea groups (model Figure 4C), a totally different behavior is observed (Figure 3). In addition to the formation of extended "pure" tapes (five+), pentamers, tetramers, trimers, dimers, and even single **T2** molecules are dispersed in the **C14-12** matrix and mixed lamellae are formed.

The two-dimensional phase behavior of the other mixtures varies between both extremes (Figure 2).

The 1:1 ratio of **T2/CX-12** in solution is not exactly reflected in the monolayer composition, which ranges from 0.8 to 3.2 for the different systems measured.[54] However, this deviation from the solution composition is small compared to other mixtures investigated.[33, 37, 40] This indicates that **T2** and **CX-12** show very similar two-dimensional nucleation behavior, growth, and interaction with the graphite support. The minimum average lamella length ranges between 15 and 21 molecules.[54, 55]

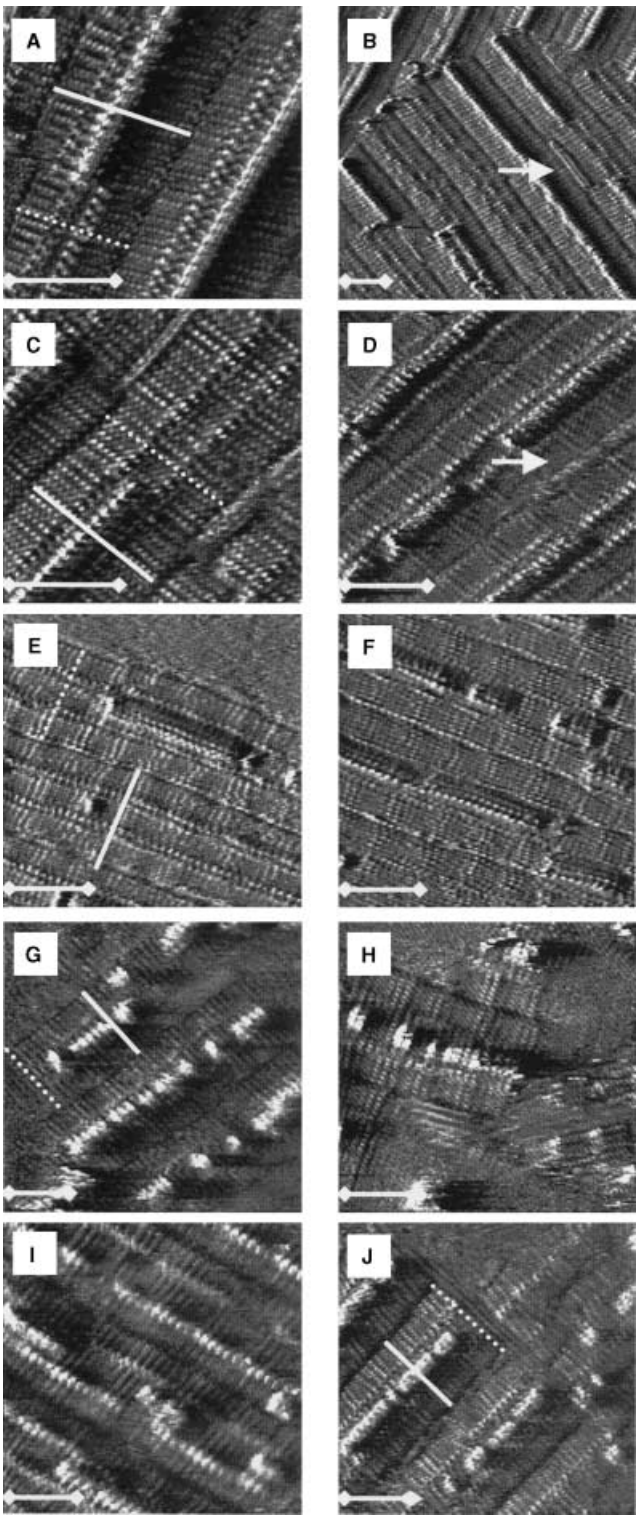

Figure 2. STM images of the mixtures. Solid (dashed) lines reflect the length, measured perpendicular to the "lamella" axis, of **T2** (**CX-12**) molecules. A, B) **T2/C6-12** mixture. C, D) **T2/C9-12** mixture. E, F) **T2/C12-12** mixture. G, H) **T2/C15-12** mixture. I, J) **T2/C16-12** mixture. The scale bar measures 4 nm.

Quantitative analysis: The images of the mixed systems were analyzed in terms of the size of the **T2** aggregates formed, and the histogram representing this analysis is shown in Figure 5A.[56] The histogram shows the average percentage of monomers, dimers, trimers, tetramers, pentamers, and five+ observed. The histogram reveals a clear size-related tendency: the monomer (five+) content increases (decreases) from **C6-12** to **C14-12** and decreases (increases) with increasing spacer length (**X** > 14). If the difference in spacer length and 14 is ~5 carbon atoms (i.e. **T2/C6-12**; **T2/C9-12**), the **T2** and **CX-12** molecules do not mix, which is reflected by the (almost) complete absence of **T2** monomers and small aggregates. If

0947-6539/03/0905-1200 $ 20.00+.50/0 *Chem. Eur. J.* **2003**, *9*, No. 5

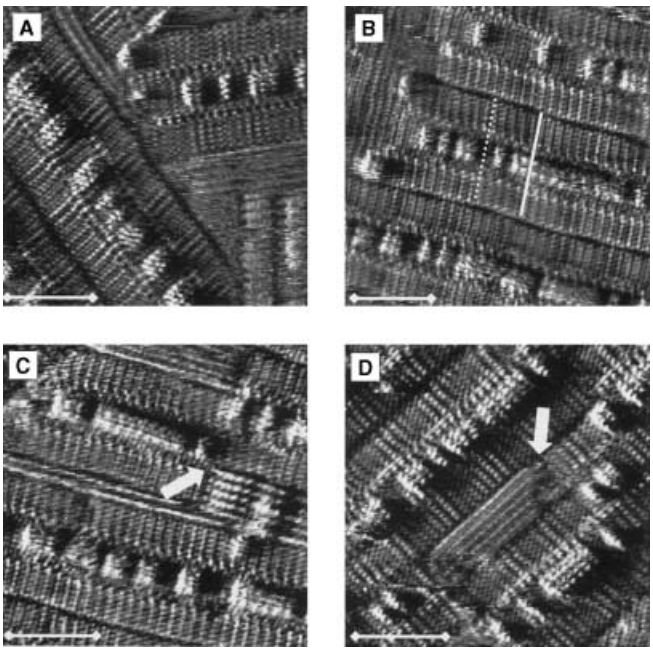

Figure 3. STM images of the **T2/C14-12** mixture. Solid (dashed) lines reflect the length, measured perpendicular to the "lamella" axis, of **T2** (**C14-12**) molecules. The molecules "mix" very well. A, B) The molecules are organized in lamellae. Different domains meet in A. C, D) Because of the molecular symmetry, molecules can easily shift by ⅓ of the molecule length (model Figure 4 D), creating defects indicated by arrows. Depending on the size of these defects, they can contain immobilized molecules, such as **T2** in C, or diffusing ones, such as in D, indicated by white arrows. The scale bar measures 4 nm.

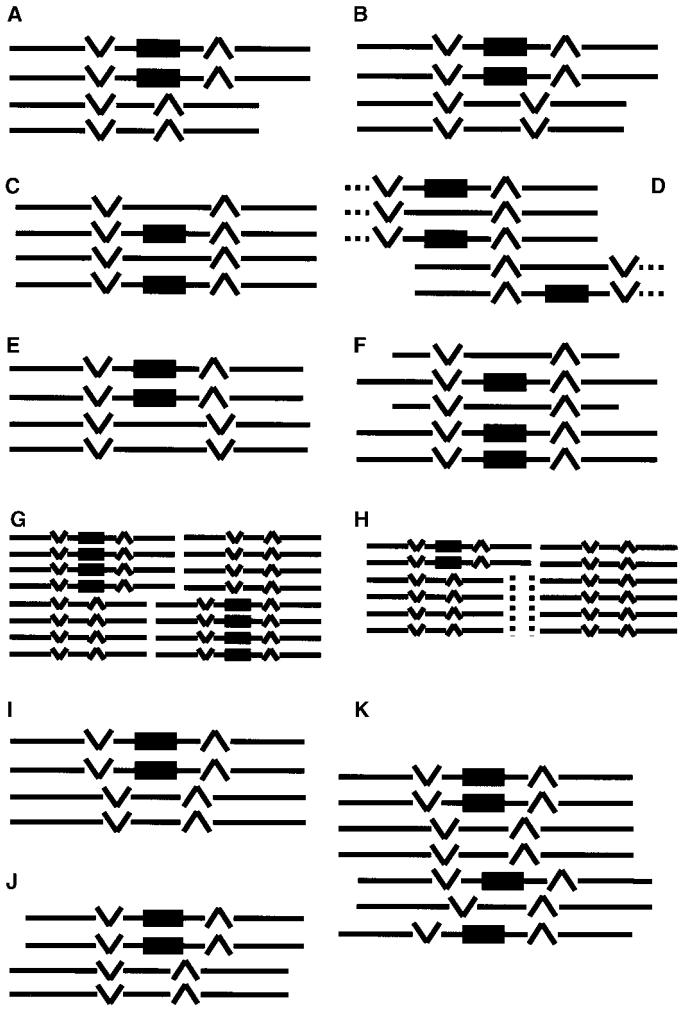

Figure 4. Schematic representation of the two-dimensional ordering of **T2** and **CX-Y** molecules within the same "lamella". The lines reflect the alkyl chains. The black box represents the bisthiophene unit. The "V" or "Λ"-shaped symbols reflect the position and the orientation of the urea groups. The point of these symbols corresponds to the carbonyl groups. The slight nonlinear shape ("zigzag"-like or "bow"-like corresponds to an even or odd number of carbon atoms in the spacer) of the molecules is neglected. A) **T2/C6-12** mixture. B) **T2/C9-12** mixture. C, D) **T2/C14-12** mixture. E) **T2/C15-12** mixture. F) **T2/C14-6** mixture. G, H) How to accommodate for different "block" sizes: molecules from the adjacent lamella are shifted to allow for an efficient packing efficiency (G); defects are created, filled by molecules oriented perpendicular to the adjacent ones (H). I, J, K) Possible interactions in a **T2/C15-8** mixture.

the difference in spacer length and 14 is smaller (i.e. **T2/C12-12**; **T2/C15-12**; **T2/C16-12**), mixtures of **T2** with **CX-12** show, in addition to the formation of large aggregates (five+), a substantial contribution of monomers and small aggregates. The mixture of **T2** and **C14-12** shows maximum mixing, as this system contains the largest relative amount of monomers and the smallest amount of five+ aggregates.

Note that a straightforward interpretation of the histogram mentioned above in terms of the tendency of the different mixtures toward phase separation is only valid if the average lamella length and co-deposition ratio are identical for all the mixtures, which is not the case.[54] However, the differences are relatively small. In addition, for a randomly intermixing system, the ratio of monomer versus large-aggregate population will decrease for both increasing average lamella length and increasing **T2/CX-12** ratio, and vice versa. Because both the co-deposition ratio and average lamella length are smaller in **T2/C15-12** compared to **T2/C14-12**, one would expect a larger monomer versus large-aggregate ratio for **T2/C15-12**; however, this is contradicted by the experimental results. This shows that the trend for phase separation deduced from the histogram is not an artefact caused by differences in average lamella length or co-deposition ratio for the different mixtures.

Simulation: To investigate whether the mixing of **T2** and **C14-12** reflects ideal behavior, we compared the experimental results of the **T2/C14-12** mixture with a simulation giving relative amounts of "*n*-mers", assuming that the mixing is under pure statistical control. In this simulation, the lamella length was kept fixed to 19 molecules, which equals the average experimental lamella length for the **T2/C14-12** mixtures.[54] During the simulations, the average **T2** content was also kept fixed according to the experimental value (58%). The histogram with the simulated values and the experimental data is given in Figure 5 B. The experimental and simulated data show good resemblance given the approximations used in the simulation. However, there is a higher preference to form five+ aggregates than simulated.[55] This is probably the result of interactions between the thiophene rings, which slightly favor neighboring **T2** molecules. Nevertheless, the comparison of the data shows that there is very good mixing between **T2** and **C14-12**.

  0947-6539/03/0905-1201 $ 20.00+.50/0

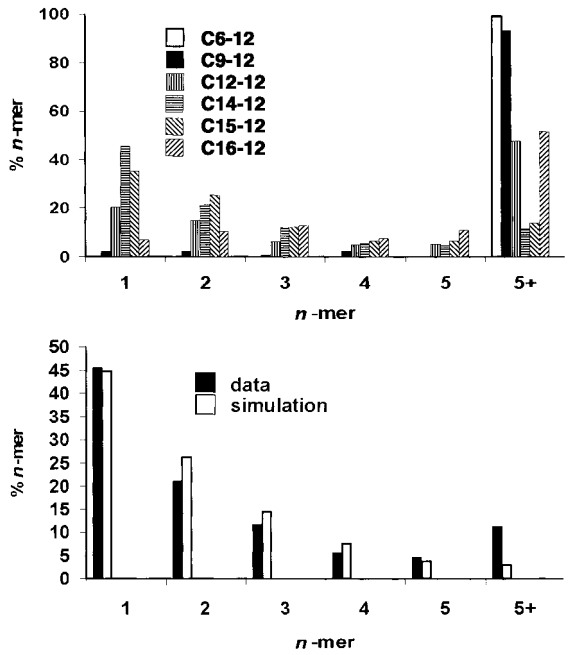

Figure 5. A) Histogram reflecting the relative content of **T2** monomers, dimers, trimers, tetramers, pentamers, and five+ clusters in the mixtures investigated. B) Histogram comparing the **T2**/**C14-12** experimental data with a simulation (see text).

Phase-separation versus statistical mixing: What drives these molecules to "mix" or "phase-separate" in two dimensions? In order to address these questions, we need to explore the intermolecular interactions in detail. The first thing to consider is why these molecules order into lamellae. The formation of lamellae is the best way to realize an optimum packing efficiency for this kind of compound that has a rather extended shape with long alkyl chains. For instance, *n*-alkanes (e.g. $C_{24}H_{50}$) are known to arrange in lamellae and form a crystalline phase.[23] Only very long alkyl chains (e.g. $C_{192}H_{386}$) show a tendency to form a quasinematic phase.[57] The compounds under investigation have two urea groups, allowing strong intermolecular hydrogen bonding. In combination with the "molecular-shape complementarity", it should not come as a surprise that lamella formation is favored.

In the mixtures, the molecules will also order in such a way as to optimize the intermolecular interactions, that is, to optimize the packing efficiency, the van der Waals interactions, and to allow, where possible, the formation of hydrogen bonds. The properties of the molecules in the mixtures discussed above are similar. All these molecules consist of two dodecyl urea groups. They only differ in the length (**CX-12**) or nature of the spacer (alkyl or bisthiophene). The dodecyl urea groups allow optimal van der Waals and hydrogen-bonding interactions between **T2** and **CX-12** molecules in a stack. Therefore, the terminal methyl groups at one side of the lamellae are found to be in line.

The **T2**/**C14-12** mixture is the only system where the length of the components is identical, and the spacer length of **T2** and **C14-12** is also the same. As a result, this is the only mixture where both dodecyl urea groups can be involved in optimal intercomponent hydrogen bonding. Comparison of the experimental data with the simulation has demonstrated the high degree of complementarity between **T2** and **C14-12**, leading to an almost ideal statistical two-dimensional mixing. Apparently, the bisthiophene unit does not affect the two-dimensional ordering significantly. Therefore, the **T2** molecules can safely be used as probes to study the two-dimensional phase behavior.

For all other systems investigated, only one of the hydrogen bonds between **T2** and **CX-12** can be maintained, as the terminal alkyl chain length is identical although the alkyl spacer length is different. Even increasing the length of the alkyl spacer with one methylene group (**C15-12**) induces phase-separation. If the difference is more than five methylene groups, the phase separation is maximal (no isolated **CX-12** molecules are observed). The difference in molecular length, leading to less favorable van der Waals interactions, in combination with the need for optimal hydrogen bonding, drives the molecules in **T2**/**CX-12** mixtures (**X** + 14) to phase separation.

Odd–even effect: Both for **T2** and **C14-12**, the alkyl spacer contains an even number of atoms linking both urea groups. Hence, in both molecules the urea groups point in opposite directions. In Figure 3B for instance, the z-shape of **C14-12**, indicating the orientation of the urea groups, can easily be distinguished; the urea groups are well-resolved and the transition between **C14-12** and **T2** molecules occurs seamlessly (model Figure 4C). As stated above, optimal hydrogen bonding between **C14-12** and **T2** is expected to take place.

The spacer of **C15-12** is not only longer, both urea groups are now directed in the same direction (model Figure 4E), making the formation of ideal hydrogen bonds between **T2** and **C15-12** difficult. Given the assumption that only one urea group is involved in hydrogen bonding, it came as a surprise that **T2** and **C15-12** mix rather well (histogram: Figure 5A) which emphasizes that hydrogen bonding is an important factor, although it is not the only factor driving the extent of phase separation in these systems.

Monolayer defects: As a result of the difference in width between the **T2** blocks and **CX-12** blocks, resulting in phase separation, monolayer defects are created that may give rise to uncovered areas. This is energetically unfavorable, and the physisorbed monolayers tend to avoid "empty" space in these mixtures in two different ways: 1) molecules from the adjacent lamella can shift in order to fill up the gap (case 1, model Figure 4G). This does not happen that often (see below), a nice illustration can be found in Figure 6D. In the upper part of that image, at the boundary between different blocks, the molecules are arranged in such a way that a close packing is achieved. 2) The gap is filled by molecules which are oriented perpendicular to the molecules in the adjacent lamellae (**T2** or **CX-12** or 1-octanol) (case 2, model Figure 4H). Examples can be found in Figure 2B, D (arrow). Quite often, no molecular or submolecular resolution is obtained in these defect areas, which is attributed to the mobility of the molecules in these gaps. This increase in mobility has several reasons: often neither the width nor the length of the defect area allows the optimal tight packing of the molecules. In addition, as the molecules are oriented

  0947-6539/03/0905-1202 $ 20.00+.50/0 *Chem. Eur. J.* **2003**, *9*, No. 5

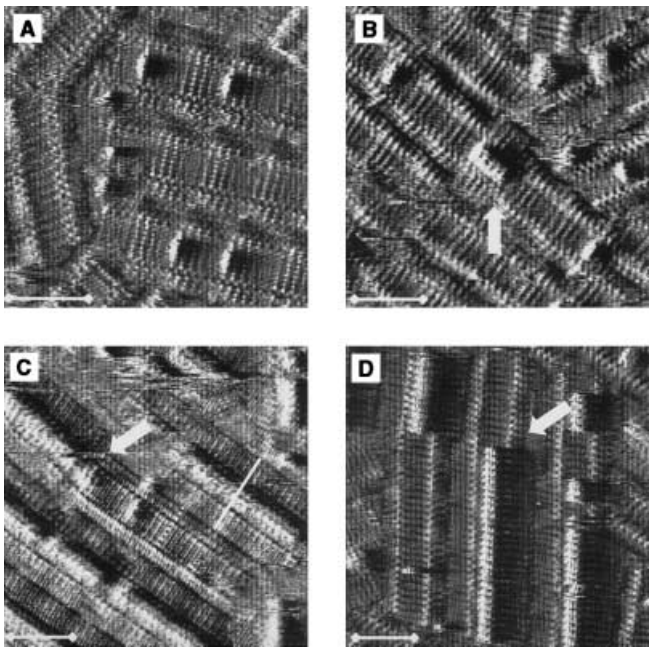

Figure 6. STM images of the **T2**/**C14-6** mixture. Solid (dashed) lines reflect the length, measured perpendicular to the "lamella" axis, of **T2** (**C14-6**) molecules. A) Isolated **T2** molecules in the **C14-6** matrix. B) Isolated molecules and some small "clusters": a pentamer is located in the center (arrow). C) Hydrogen bonding domination at the boundary between a **T2** and **C14-6** block (arrow). D) Efficient monolayer packing at a domain boundary (arrow). The scale bar measures 4 nm.

perpendicular to the adjacent molecules, the alkyl chains are not aligned parallel to one of the major graphite axes of the underlying graphite support. Therefore, the interactions between those alkyl chains and the graphite support are smaller. Case 2 occurs more often than case 1, which might seem somewhat surprising. However, one should keep in mind that along pure blocks, intermolecular hydrogen bonding is very strong and the formation of "straight" lamellae is favored. Occasionally, similar defects are formed but for another reason. Although the formation of "straight" lamellae is favored, it can happen that molecules laterally shift with respect to each other by roughly ⅓ of the molecule length, as is shown in Figure 3C, D (arrows) for the **T2**/**C14-12** mixture. At such a dislocation, hydrogen bonding is still possible between urea groups (model Figure 4D). This type of dislocations often induces monolayer defects with a defined width, but not with a defined length. For instance, in Figure 3C, five **T2** molecules are trapped and oriented perpendicular to the adjacent molecules. Because of the size of the defect, the molecules are immobilized. In the same image, the two long lines running from left to right are caused by mobile molecules. In Figure 3D (center), the trapped molecules are not immobilized and individual molecules are not visible.

T2/C14-6 versus T2/C14-12

To evaluate the importance of hydrogen bonding versus molecule length with respect to the two-dimensional phase behavior, a mixture of **T2** with **C14-6**, a bisurea derivative containing hexylurea side chains, was investigated. The design of this molecule allows, in principle, the optimum formation of hydrogen bonds and this should favor mixing. The difference in length between **T2** and **C14-6** (12 methylene groups) should promote phase separation. Figure 6 shows some representative images of this mixture. The **C14-6** molecules can easily be identified by the short terminal hexyl chains and the long spacer connecting both urea groups. As for the other systems, **T2** molecules are also codeposited. In Figure 6A, a few isolated **T2** molecules are visible. The bright structures, corresponding to the bisthiophene unit, are centered and located between the urea groups of adjacent **C14-6** molecules. This indicates that the isolated **T2** molecules are anchored by hydrogen bonding. As a result, the terminal methyl groups of the dodecyl chains of the **T2** molecules cannot be in line with the terminal methyl groups of the hexyl chains of the **C14-6** molecules. In addition to isolated **T2** molecules, in Figure 6B, some small clusters of **T2** can be observed (model Figure 4F). In the center of the image, a **T2** pentamer is trapped in a **C14-6** lamella. In this case, the dodecyl groups can easily be resolved and they are fully absorbed on the graphite substrate. Evidently, in terms of packing efficiency, this is not the best "solution"; however, it demonstrates the effect of hydrogen bonding on the two-dimensional ordering. Another clear example is given in Figure 6C. This image shows some pure **T2** and **C14-6** blocks. Of special interest is the area indicated with the arrow where a **T2** block meets a **C14-6** block. The **C14-6** block runs parallel to the adjacent **T2** lamellae, but the **T2** block does not. At the boundary between the **T2** and the **C14-6** block, the **T2** molecule complements well with the adjacent **C14-6** molecule and forms hydrogen bonds. However, because of the adjacent **T2** lamella at its lower side, there is no space for the dodecyl groups. As a result, the molecules in that **T2** block gradually shift "upwards" to accommodate space for all the dodecyl groups, while maintaining hydrogen bonding. The examples illustrate the importance of hydrogen-bond formation, which is also confirmed by the monolayer formation, as shown in Figure 6D. Instead of isolated **T2** molecules, pure strands of **T2** and **C14-6** are formed. Nevertheless, the ordering of the molecules allows a seamlessly perfect fit of the hydrogen bonds on account of the small relative shift of the lamellae, which creates an optimum packing efficiency.

Based upon the large difference in size, **T2** and **C14-6** should exclusively show phase separation (**T2**/**C6-12** shows 100% phase separation!). However, as shown in the images, isolated **T2** molecules and clusters are observed. If, in molecules with identical spacer length, all the urea groups can be involved in hydrogen bonding, the latter noncovalent interaction dominates the two-dimensional phase behavior.

Phase separation in molecules with identical size

So far, except for the **T2**/**C14-12** mixture, the components differ in size. Although it was shown that hydrogen bonding is definitely important (and dominant for systems with a tetradecyl spacer: all urea groups are involved in hydrogen bonding) in the two-dimensional phase behavior, it was clearly demonstrated that increasing the difference between the **T2** and **CX-12** spacer length promotes phase separation.

  0947-6539/03/0905-1203 $ 20.00+.50/0

In order to probe exclusively the effect of hydrogen bonding, mixtures of **T2** and bisurea derivatives were studied with (almost) identical molecule length, but with differing positions of the urea groups. To realize this, symmetrical bisurea derivatives were studied with pentadecyl alkyl chains and an octyl or nonyl spacer group, with a total of 38 (**C8-15**) or 39 (**C9-15**) carbon atoms, respectively. In principle, three different situations are possible for the mixtures (model Figure 4I–K). Situation 1) Phase separation (model Figure 4I): the molecules stack in rows with alternating "blocks" of **T2** and **CX-15**. Both types of molecules are perfectly aligned, lamellae are "straight" and hydrogen bonding at the boundary between **T2** and **CX-15** blocks is not possible. Situation 2) - Phase separation (model Figure 4J): the molecules align in rows and phase separate, but in such a way that one hydrogen bond can be formed at the boundary between **T2** and **CX-15** lamellae. Situation 3) Mixing with and without formation of hydrogen bonds (model Figure 4 K). Figure 7 shows the STM

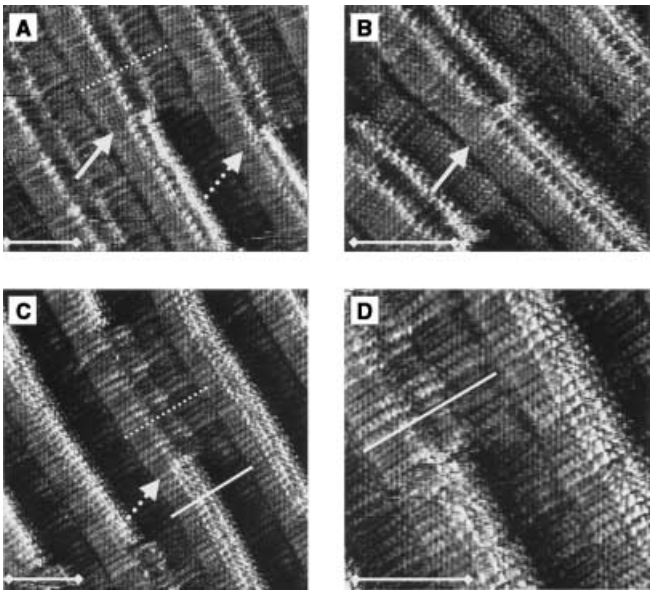

Figure 7. STM images of the **T2/C15-Y** mixture. Solid (dashed) lines reflect the length, measured perpendicular to the "lamella" axis, of **T2** (**C15-Y**) molecules. A, B) **T2/C15-8** mixture. C, D) **T2/C15-9** mixture. The solid arrow refers to "situation 1": see text and model Figure 4I. The dashed arrow refers to "situation 2": see text and model Figure 4J. The scale bar measures 4 nm.

images of **T2/C8-15** and **T2/C9-15** mixed monolayers. Without any exceptions, complete phase separation is observed, regardless of the C8 or C9 spacer length. As anticipated, the molecules stack in rows with alternating "blocks" of **T2** and **CX-15**. Close inspection of Figure 7 reveals that both situation 1 (model Figure 4I) and situation 2 (model Figure 4J) occur. For instance, in the lamella in the center of Figure 7A and B (solid arrow), it is clear that the urea groups of the **T2** molecules are not in line with the urea groups of the **C8-15** block. For the right lamella in Figure 7A (dashed arrow), the left row of urea groups of the **T2** and C8-15 block appear to be in line. It is more difficult to distinguish between both situations for the **T2/C9-15** mixture; however, in the images in Figure 7C and D, urea groups tend to be in line. It can be concluded that both situation 1 and situation 2 are possible while situation 3 does not occur. For situation 1, "straight" lamellae are formed, limiting the number of monolayer defects formed, at the expense of hydrogen-bond formation. For situation 2, one hydrogen bond can be formed at the domain boundary between a **T2** and **C8-15** block, inducing a small lateral offset, which could potentially lead to an enhanced formation of monolayer defects. The absence of situation 3 illustrates that both types of molecules do not "fit" well together and that, in absence of hydrogen bonding "glue", phase separation occurs.

Conclusion

This study aimed to investigate the relationship between molecular structural differences—length, location of functional groups, odd–even effects, shape complementarity—and the two-dimensional phase behavior.

As expected, phase separation is promoted by an increase in the difference in molecule length while randomly intermixing is optimal when the length of both components is identical. In addition, the presence and the location of the hydrogen-bonding units in the molecules plays an important role. Hydrogen bonding can counteract the effect of the difference in molecule length on the two-dimensional phase behavior.

Although it is not possible to control the size of the aggregates, it is possible to influence to a large extent the phase behavior leading to optimal intermixing or phase separation by paying attention to the possible intermolecular interactions.

Experimental Section

Materials and methods: All solvents were dried according to standard procedures. Starting materials were purchased from Aldrich or Acros. ^{1}H NMR spectra were recorded on a Varian VXR-300 spectrometer (at 300 MHz) in TFA + CD_3OD (10% v/v), chemical shifts are given in ppm relative to methanol ($\delta = 3.35$). ^{13}C NMR spectra were recorded on a Varian VXR 300 spectrometer (at 75.48 MHz) in TFA + D_2O (10% v/v), chemical shifts are given relative to TFA ($\delta = 154.3$). The splitting patterns in the ^{1}H NMR spectra are designated as follows: s (singlet), d (doublet), t (triplet), m (multiplet), br (broad). Melting points were measured on Stuart scientific SMP1 apparatus. Infrared spectra were recorded on a Nexus FTIR spectrometer. Elemental analyses were carried out in the Microanalytical department of the Stratingh Institute, University of Groningen (The Netherlands).

The synthesis of compounds **C12-12**, **C9-12**, **C6-12**, and the bisthiophene (**T2**) (Scheme 1) has been reported.[51, 58] The other linear bisurea compounds were synthesized by reaction of α,ω-diamines with the appropriate isocyanates. Diaminooctane and diaminononane are commercially available. Diaminotetradecane, diaminopentadecane, and diaminohexadecane were synthesized from the corresponding diols, in a sequence that converts them to the dibromides,[59] then to the diazides,[60] which were then reduced to the corresponding diamines.[61]

1-Hexyl-3-[14-(3-hexylureido)tetradecyl]urea (C14-6): Hexylisocyanate (250 mg, 2 mmol) was slowly added to a stirred solution of 1,14-diaminotetradecane (180 mg, 0.8 mmol) in hot toluene (20 mL). An off-white suspension formed immediately. After stirring for 2 h, the mixture was poured into diethyl ether, and the product precipitated as a white solid. After sonication for 1 h, the precipitate was collected by filtration and washed with diethyl ether. The product could be purified by repeated precipitation from *p*-xylene. Yield: 0.3 g (0.6 mmol, 75%); m.p. 163–

0947-6539/03/0905-1204 $ 20.00+.50/0 *Chem. Eur. J.* **2003**, *9*, No. 5

165 °C (decomp); ^{1}H NMR (300 MHz, TFA + CD_3OD): $\delta = 2.70$ (t, $^3J(H,H) = 6.9$ Hz, 8H), 1.01 (m, 8H), 0.67(m, 32H), 0.23 ppm (s, 6H); ^{13}C NMR (75.48 MHz, TFA + D_2O): $\delta = 152.5$, 35.6, 24.4, 22.8, 22.7, 22.6, 22.3, 21.9, 19.7, 19.4, 15.5, 6.0 ppm; IR (KBr): $\tilde{\nu} = 3336$, 1614, 1576 cm^{-1}; $C_{28}H_{58}N_4O_2$ (482.79): *m*/*z*: 482; elemental analysis (%) calcd: C 69.66, H 12.11, N 11.60; found: C 69.53, H 12.02, N 11.52.

1-Dodecyl-3-[14-(3-dodecylureido)tetradecyl]urea (C14-12): This was synthesized as described for **C14-6**, starting from 1,14-diaminotetradecane (200 mg, 0.8 mmol) and dodecylisocyanate (400 mg, 1.9 mmol). Yield: 0.34 g (65%); m.p. 159–160 °C (decomp); ^{1}H NMR (300 MHz, TFA + CD_3OD): $\delta = 2.71$ (t, $^3J(H,H) = 6.6$ Hz, 8H), δ 1.02 (m, 8H), 0.67 (m, 56H), 0.23 ppm (s, 6H); ^{13}C NMR (75.48 MHz, TFA + D_2O,): $\delta = 36.1$, 25.9, 23.5, 23.3, 22.9, 22.6, 20.4, 16.5, 7.0 ppm; IR (KBr): $\tilde{\nu} = 3336$, 1611, 1574 cm^{-1}; elemental analysis (%) calcd for $C_{40}H_{82}N_4O_2$ (651.12): C 73.79, H 12.69, N 8.60; found: C 73.60, H 12.64, N 8.37.

1-Dodecyl-3-[15-(3-dodecylureido)pentadecyl]urea (C15-12): This was synthesized as described for **C14-6**, starting from 1,15-diaminopentadecane (200 mg, 0.8 mmol) and dodecylisocyanate (400 mg, 1.9 mmol). Yield: 0.38 g (71%); m.p. 162–164 °C (decomp); ^{1}H NMR (300 MHz, TFA + CD_3OD): $\delta = 2.71$ (t, $^3J(H,H) = 6.6$ Hz, 8H), 1.02 (m, 8H), 0.67 (m, 58H), 0.22 ppm (s, 6H); ^{13}C NMR (75.48 MHz, TFA + D_2O): $\delta = 152.7$, 35.7, 23.0, 22.9, 22.8, 22.4, 22.1, 19.9, 16.0, 6.4 ppm; IR (KBr): $\tilde{\nu} = 3336$, 1611, 1574 cm^{-1}; $C_{41}H_{84}N_4O_2$ (665.14): *m*/*z*: 665.8; elemental analysis (%) calcd C 74.04, H 12.73, N 8.42; found: C 73.88, H 12.69, N 8.45.

1-Dodecyl-3-[16-(3-dodecylureido)hexadecyl]urea (C16-12): This was synthesized as described for **C14-6**, starting from 1,16-diaminohexadecane (200 mg, 0.8 mmol) and dodecylisocyanate (400 mg, 1.9 mmol). Yield: 430 mg (78%); m.p. 164–165 °C (decomp); ^{1}H NMR (300 MHz, TFA + CD_3OD): $\delta = 2.71$ (t, $^3J(H,H) = 6.6$ Hz, 8H), 1.02 (m, 8H), 0.67 (m, 60H), 0.23 ppm (s, 6H); ^{13}C NMR (75.48 MHz, TFA + D_2O): $\delta = (152.7)$, 35.5, 25.2, 22.9, 22.8, 22.4, 22.3, 22.1, 19.9, 16.0, 6.3 ppm; IR (KBr): $\tilde{\nu} = 3331$, 1612, 1569 cm^{-1}; elemental analysis (%) calcd for $C_{41}H_{84}N_4O_2$ (679.17): C 74.28, H 12.76, N 8.25; found: C 74.09, H 12.81, N 8.13.

1-Isocyanatopentadecane: Palmitoyl chloride (5 g, 0.018 mol) was dissolved in *p*-xylene (40 mL). Sodium azide (1.5 g, 0.023 mol) was added. The reaction mixture was heated at reflux for 2 h under a continuous flow of nitrogen, after which conversion to the isocyanate was complete. The hot reaction mixture was filtered to remove insoluble residue. The solvent was removed in vacuo to yield the product as a semisolid material. Yield: 4.5 g (0.018 mol, 99%); ^{1}H NMR (300 MHz, $CDCl_3$): $\delta = 3.22$ (t, $^3J(H,H) =$ 6.6 Hz, 2H), 1.55 (m, 2H), 1.21 (m, 24H), 0.82 ppm (t, 3H); ^{13}C NMR (75.48 MHz, $CDCl_3$, TMS): $\delta = 134.0$, 42.1, 31.2, 30.5, 29.9, 29.8, 29.4, 28.8, 26.4, 22.1, 20.2, 16.0, 13.5 ppm.

1-Pentadecyl-3-[8-(3-pentadecylureido)octyl]urea (C15-8): This was synthesized as described for **C14-6**, starting from 1-isocyanato-pentadecane (0.4 g, 1.6 mmol) and 1,8-diaminooctane (100 mg, 0.7 mmol) in hot toluene (20 mL). Yield: 380 mg (85%); m.p. 167–169 °C (decomp); ^{1}H NMR (300 MHz, TFA + CD_3OD): $\delta = 2.70$ (t, $^3J(H,H) = 6.6$ Hz, 8H), 1.02 (m, 8H), 0.66 (m, 56H), 0.22 ppm (s, 6H); ^{13}C NMR (75.48 MHz, TFA + D_2O): $\delta = (152.7)$, 36.3, 26.1, 23.7, 23.6, 23.5, 23.4, 23.1, 22.9, 22.8, 20.6, 20.5,16.7, 7.3 ppm; IR (KBr): $\tilde{\nu} = 3336$, 1611, 1576 cm^{-1}; $C_{40}H_{82}N_4O_2$ (651.12): *m*/*z*: 651.6; elemental analysis (%) calcd: C 73.79, H 12.69, N 8.60; found: C 73.41, H 12.57, N 8.35.

1-Pentadecyl-3-[9-(3-pentadecylureido)nonyl]urea (C15-9): This was synthesized as described for **C14-6**, starting from 1-isocyanato-pentadecane (0.35 g, 1.4 mmol) and 1,9-diaminononane (100 mg, 0.65 mmol) in hot toluene (20 mL). Yield: 390 mg (90%); m.p. 161–163 °C; ^{1}H NMR (300 MHz, TFA + CD_3OD): $\delta = 2.72$ (t, $^3J(H,H) = 6.6$ Hz, 8H), 1.03 (m, 8H), 0.67 (m, 58H), 0.24 ppm (s, 6H); ^{13}C NMR (75.48 MHz, TFA + D_2O): $\delta = (153.1)$, 35.9, 25.8, 23.5, 23.4, 23.3, 23.2, 23.1, 22.8, 22.7, 20.2,16.4, 7.0 ppm; IR (KBr): $\tilde{\nu} = 3336$, 1611, 1574 cm^{-1}; $C_{41}H_{84}N_4O_2$ (665.14): *m*/*z*: 665.6; elemental analysis calcd: C 74.04, H 12.73, N 8.42; found: C 73.68, H 12.75, N 8.39.

STM: Prior to imaging, all compounds under investigation were dissolved in 1-octanol and a drop of this solution was applied to a freshly cleaved surface of highly oriented pyrolytic graphite (HOPG). The molar ratio in solution of the mixtures of **T2** and **CX-Y** was 1:1. The STM images were acquired in the variable-current mode (constant height) under ambient conditions with the tip immersed in the liquid. In the acquired STM images, white corresponds to the highest and black to the lowest measured tunneling current. STM experiments were performed with a Discoverer scanning tunneling microscope (Topometrix Inc., Santa Barbara, CA) along with an external pulse/function generator (Model HP 8111 A), with negative sample bias. Tips were electrochemically etched from Pt/Ir wire (80%/20%, diameter 0.2 mm) in a 2 N KOH/6 N NaCN solution in water.

The experiments were repeated in several sessions with different tips to check for reproducibility and to avoid artifacts. Different settings for the tunneling current and the bias voltage were used, ranging from 0.3 nA to 1.0 nA and -10 mV to -1.5 V, respectively. All STM images contain raw data and are not subjected to any manipulation or image processing.

Acknowledgement

The authors thank the DWTC, through IUAP-V-03, the Institute for the promotion of innovation by Sciences and Technology in Flanders (IWT). ESF SMARTON made the Leuven–Groningen collaboration possible. S.D.F. is a postdoctoral fellow of the Fund for Scientific Research-Flanders. J.v.E. gratefully acknowledges the Royal Academy of the Netherlands for a fellowship. M.L. is an Erasmus student from Karlstad University (Sweden). B.V. is an Erasmus student from University of Groningen (The Netherlands).

[1] *Handbook of Microlithography, Micromachining, and Microfabrication* (Ed.: P. Rai-Choudhury), SPIE Optical Engineering Press, London, **1997**.
[2] Y. Xia, G. M. Whitesides, *Angew. Chem.* **1998**, *110*, 568–594; *Angew. Chem. Int. Ed. Engl.* **1998**, *37*, 550–575.
[3] G. Binnig, H. Rohrer, C. Gerber, E. Weibel, *Phys. Rev. Lett.* **1982**, *49*, 57–61.
[4] G. Binnig, C. F. Quate, C. Gerber, *Phys. Rev. Lett.* **1986**, *56*, 930–933.
[5] Y.-T. Kim, A. J. Bard, *Langmuir* **1992**, *8*, 1096–1102.
[6] C. B. Ross, L. Sun, R. M. Crooks, *Langmuir* **1993**, *9*, 632–636.
[7] G.-Y. Liu, S. Xu, Y. Qian, *Acc. Chem. Res.* **2000**, *33*, 457–466.
[8] W. T. Müller, D. L. Klein, T. Lee, J. Clarke, P. L. McEuen, P. G. Schultz, *Science* **1995**, *268*, 272–273
[9] R. Maoz, S .R. Cohen, J. Sagiv, *Adv. Mat.* **1999**, *11*, 55–61.
[10] *Comprehensive supramolecular chemistry* (Eds: J. L. Atwood, J. E. D. Davies, D. D. MacNicol, F. Vögtle), Pergamon, New York, **1996**.
[11] A. Ulman, *Chem. Rev.* **1996**, *96*, 1533–1554, and references therein.
[12] C. D. Bain, G. M. Whitesides, *J. Am. Chem. Soc.* **1988**, *110*, 6560–6561.
[13] P. A. Lewis, Z. J. Donhauser, B. A. Mantooth, R. K. Smith, L. A. Bumm, K. F. Kelly, P. S. Weiss, *Nanotechnology* **2001**, *12*, 231–237, and references therein.
[14] K. Tamada, M. Hara, H. Sasabe, W. Knoll, *Langmuir* **1997**, *13*, 1558–1566.
[15] S. J. Stranick, S. V. Atre, A. N. Parikh, M. C. Wood, D. L. Allara, N. Winograd, P. S. Weiss, *Nanotechnology* **1996**, *7*, 438–442.
[16] R. K. Smith, S. M. Reed, P. A. Lewis, J. D. Monnell, R .S. Clegg, K. F. Kelly, L. A. Bumm, J. E. Hutchison, P. S. Weiss, *J. Phys. Chem. B* **2001**, *105*, 1119–1122.
[17] T. Yokoyama, S. Yokoyama, T. Kamikado, Y. Okuno, S. Mashiko, *Nature* **2001**, *413*, 619–621.
[18] M. Böhringer, K. Morgenstern, W.-D. Schneider, R. Berndt, F. Mauri, A. De Vita, R. Car, *Phys. Rev. Lett.* **1999**, *83*, 324–327.
[19] J. Weckesser, A. De Vita, J. V. Barth, C. Cai, K. Kern, *Phys. Rev. Lett.* **2001**, *87*, 6101–6104.
[20] A. Dmitriev, N. Lin, J. Weckesser, J. V. Barth, K. Kern, *J. Phys. Chem. B* **2002**, *106*, 6907–6912.
[21] M. O. Lorenzo, C. J. Baddeley, C. Muryn, R. Raval, *Nature* **2000**, *404*, 376–379.
[22] G. C. McGonical, R. H. Bernhardt, D. J. Thomson, *Appl. Phys. Lett.* **1990**, *57*, 28–30.
[23] J. P. Rabe, S. Buchholz, *Science* **1991**, *253*, 424–427.
[24] J. Frommer, *Angew. Chem.* **1992**, *104*, 1325–1357; *Angew. Chem. Int. Ed. Engl.* **1992**, *31*, 1298–1328.
[25] D. M. Cyr, B. Venkataraman, G. W. Flynn, *Chem. Mater.* **1996**, *8*, 1600–1615.
[26] L. C. Giancarlo, G. W. Flynn, *Annu. Rev. Phys. Chem.* **1998**, *49*, 297–336.

  0947-6539/03/0905-1205 $ 20.00+.50/0

[27] S. De Feyter, A. Gesquière, M. M. Abdel-Mottaleb, P. C. M. Grim, F. C. De Schryver, C. Meiners, M. Sieffert, S. Valiyaveettil, K. Müllen, *Acc. Chem. Res.* **2000**, *33*, 8, 520 – 531.
[28] B. Venkataraman, J. J. Breen, G. W. Flynn, *J. Phys. Chem.* **1995**, *99*, 6608 – 6619.
[29] J.-C. Poulin, *Microsc. Microanal. Microstruct.* **1994**, *5*, 351.
[30] N. Elbel, W. Roth, E. Günther, H. von Seggern, *Surface Science* **1994**, *303*, 424 – 432.
[31] M. Hibino, A. Sumi, I.Hatta, *Thin Solid Films* **1996**, *281 – 282*, 594 – 597.
[32] F. Stevens, D. J. Dyer, D. M. Walba, *Langmuir* **1996**, *12*, 436 – 440.
[33] R. T. Baker, J. D. Mougous, A. Brackley, D. L. Patrick, *Langmuir* **1999**, *15*, 4884 – 4891.
[34] K. W. Hipps, X. Lu, X. D. Wang, U. Mazur, *J. Phys. Chem.* **1996**, *100*, 11207 – 11210.
[35] X. Lu, K. W. Hipps, X. D. Wang, U. Mazur, *J. Am. Chem. Soc.* **1996**, *118*, 7197 – 7202.
[36] N. J. Tao, *Phys. Rev. Lett.* **1996**, *76*, 4066 – 4069.
[37] F. Stevens, T. P. Beebe, *Langmuir* **1999**, *15*, 6884 – 6889.
[38] D. F. Padowitz, B. W. Messmore, *J. Phys. Chem. B* **2000**, *104*, 9943 – 9946.
[39] D. F. Padowitz, D. M. Sada, E. L. Kemer, M. L. Dougan, W. A. Xue, *J. Phys. Chem. B.* **2002**, *106*, 593 – 598.
[40] A. Gesquière, M. Abdel-Mottaleb, F. C. De Schryver, M. Sieffert, K. Müllen, *Langmuir* **1999**, *15*, 6821 – 6824.
[41] L. C. Giancarlo, G. W. Flynn, *Acc. Chem. Res.* **2000**, *33*, 491 – 501.
[42] P. Vanoppen, P. C. M. Grim, M. Rücker, S. De Feyter, G. Moessner, S. Valiyaveetil, K. Müllen, F. De Schryver, *J. Phys. Chem.* **1996**, *100*, 19636 – 19641.
[43] P. C. M. Grim, S. De Feyter, A. Gesquière, P. Vanoppen, M. Rücker, S. Valiyaveettil, G. Moessner, K. Müllen, F. C. De Schryver, *Angew. Chem.* **1997**, *109*, 2713 – 2715; *Angew. Chem. Int. Ed. Engl.* **1997**, *36*, 2601 – 2603.
[44] S. De Feyter, P. C. M. Grim, M. Rücker, P. Vanoppen, C. Meiners, M. Sieffert, S. Valiyaveettil, K. Müllen, F. C. De Schryver, *Angew. Chem.* **1998**, *110*, 1281 – 1284; *Angew. Chem. Int. Ed.* **1998**, *37*, 1223 – 1226.
[45] A. Gesquière, M. M. Abdel-Mottaleb, S. De Feyter, F. C. De Schryver, M. Sieffert, K. Müllen, A. Calderone, R. Lazzaroni, J.-L. Brédas, *Chem. Eur. J.* **2000**, *6*, 20, 3739 – 3746.
[46] K. Eichhorst-Gerner, A. Stabel, G. Moessner, D. Declercq, S. Valiyaveettil, V. Enkelmann, K. Müllen, J. P. Rabe, *Angew. Chem.* **1996**, *108*, 1599 – 1602; *Angew. Chem. Int. Ed. Engl.* **1996**, *35*, 1492 – 1495.
[47] P. Qian, H. Nanjo, T. Yokoyama, T. M. Suzuki, K. Akasaka, H. Orhui, *Chem. Commun.* **2000**, 2021 – 2022.
[48] K. W. Hipps, L. Scudiero, D. E. Barlow, M. P. Cooke, *J. Am. Chem. Soc.* **2002**, *124*, 2126 – 2127.
[49] S. B. Lei, C. Wang, S. X. Yin, C. L. Bai, *J. Phys. Chem. B* **2001**, *105*, 12272 – 12277.
[50] A. Gesquière, S. De Feyter, F. C. De Schryver, F. Schoonbeek, J. van Esch, R. M. Kellogg, B. L. Feringa, *Nano Lett.* **2001**, *1*, 4, 201 – 206.
[51] J. van Esch, S. De Feyter, R. M. Kellogg, F. De Schryver, B. L. Feringa, *Chem. Eur. J.* **1997**, *3*, 1238 – 1243.
[52] S. De Feyter, K. Grim, J. van Esch, R. M. Kellogg, B. L. Feringa, F. C. De Schryver, *J. Phys. Chem. B* **1998**, *102*, 8981 – 8987.
[53] A. Gesquière, M. M. S. Abdel-Mottaleb, S. De Feyter, F. C. De - Schryver, F. Schoonbeek, J. van Esch, R. M. Kellogg, B. L. Feringa, A. Calderone, R. Lazzaroni, J. L. Brédas, *Langmuir* **2000**, *16*, 10385 – 10391.
[54] The **T2/CX-12** deposition ratio and average lamella length are respectively 3.2 and 21.2 (**T2/C9-12**), 0.9 and 21.2 (**T2/C12-12**), 1.7 and 19.2 (**T2/C12-14**), 0.8 and 15.3 (**T2/C12-15**), and 1.4 and 15.9 (**T2/C12-16**).
[55] The average lamella length measured must be shorter than the real lamella length as borders imposed by the image size are considered to be "real" borders. This leads to an overestimation of **T2** monomer content and an underestimation of the large *n*-mers in the simulation.
[56] The number of lamellae analyzed for the different mixtures is 141 (**T2/C6-12**), 161 (**T2/C9-12**), 208 (**T2/C12-12**), 228 (**T2/C14-12**), 107 (**T2/C15-12**), and 139 (**T2/C16-12**).
[57] L. Askadskaya, J. P. Rabe, *Phys. Rev. Lett.* **1992**, *69*, 1395 – 1398.
[58] F. S. Schoonbeek, J. van Esch, B. Wegewijs, D. B. A. Rep, M. P. de Haas, T. M. Klapwijk, R. Kellogg, B. L. Feringa, *Angew. Chem.* **1999**, *111*, 1486 – 1490; *Angew. Chem. Int. Ed.* **1999**, *38*, 1393 – 1397.
[59] V. Percec, Y. Tsula, *Polym. Bull.* **1989**, *22*, 497.
[60] The diazides were synthesized from the dibromides according to the method of S. G. Alvarez, M. T. Alvararez, *Synthesis*, **1997**, 413.
[61] Catalytic reduction with H_2, over Pd/C, in EtOH.

Received: September 6, 2002 [F4397]

  0947-6539/03/0905-1206 $ 20.00+.50/0